THE JOURNAL OF PHYSICAL CHEMISTRY C
A JOURNAL OF THE AMERICAN CHEMICAL SOCIETY

pubs.acs.org/JPCC

Article

Energy-Level Alignment at Interfaces between Transition-Metal Dichalcogenide Monolayers and Metal Electrodes Studied with Kelvin Probe Force Microscopy

Pavel A. Markeev,* Emad Najafidehaghani, Ziyang Gan, Kai Sotthewes, Antony George, Andrey Turchanin, and Michel P. de Jong

Cite This: *J. Phys. Chem. C* 2021, 125, 13551−13559

Read Online

ACCESS | Metrics & More | Article Recommendations | Supporting Information

ABSTRACT: We studied the energy-level alignment at interfaces between various transition-metal dichalcogenide (TMD) monolayers, MoS_2, $MoSe_2$, WS_2, and WSe_2, and metal electrodes with different work functions (WFs). TMDs were deposited on SiO_2/silicon wafers by chemical vapor deposition and transferred to Al and Au substrates, with significantly different WFs to identify the metal−semiconductor junction behavior: oxide-terminated Al (natural oxidation) and Au (UV−ozone oxidation) with a WF difference of 0.8 eV. Kelvin probe force microscopy was employed for this study, based on which electronic band diagrams for each case were determined. We observed the Fermi-level pinning for MoS_2, while WSe_2/metal junctions behaved according to the Schottky−Mott limit. WS_2 and $MoSe_2$ exhibited intermediate behavior.

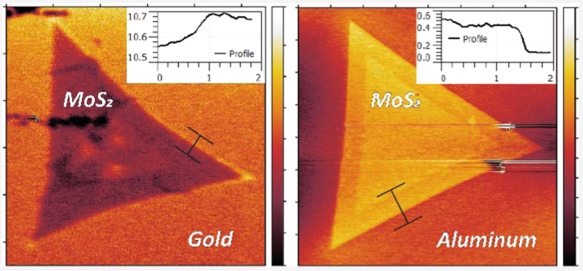

1. INTRODUCTION

The alignment of energy levels at interfaces between two-dimensional (2D) transition-metal dichalcogenides (TMDs) and metallic electrodes determines, to a large extent, the charge injection and extraction efficiency at such interfaces. Metal−semiconductor junctions have been extensively studied for a wide range of bulk semiconductors, and the Schottky barrier formed at such junctions is determined by the Schottky−Mott rule,[1,2] in combination with the distribution of interface states.[3] In the case of 2D transition-metal dichalcogenides, the TMD−metal contact area does not have a depletion region in the traditional sense, which must be taken into account for the metal−semiconductor contacts. For more than 3 layers, the behavior is approaching that of the bulk material in an exponential manner.[4−7] Conventional semiconductor (bulk) terminology is therefore not very suitable for 2D semiconductors. For example, the well-described surface states for bulk semiconductors are simply not present in 2D semiconductors, as the surfaces of these layered van der Waals materials do not exhibit dangling bonds.[8] Although edge states (one-dimensional (1D)) are present in the 2D case, these states do not have a comparable effect on the interfacial dipoles at the interfaces. However, TMDs typically exhibit gap states related to (point) defects in the lattice,[9,10] and chemical interactions at the metal/TMD interface may lead to metal-induced gap states as well, making it challenging to achieve the Schottky−Mott limit for metal/TMD contacts.[11] Contacts between TMDs and metal electrodes therefore need to be carefully engineered to achieve the desired electronic properties.[12,13]

The positions of the valence band maximum and conduction band minimum (CB) are key components for the semiconductor heterojunction design.[14] These band positions largely determine the band alignment in the heterojunction, and hence the energy barrier for charge injection and extraction.[15] The ionization energy of TMDs has been studied by the density functional theory (DFT) calculations[16−21] and experimental work, but the latter is mainly concentrated on TMD flakes located on SiO_2/Si substrates, not taking into account electrode−TMD interactions.[22−24]

In this work, we report on the energy-level alignment at interfaces between metal electrodes and several different monolayer TMDs, namely, MoS_2, $MoSe_2$, WS_2, and WSe_2. For the metal electrodes, we have chosen passivated Au and Al layers, which have significantly different work functions (WFs). This allowed us to study the effect of the metal WFs on the energy-level alignment. It is well known that, in general, the alignment of energy levels at a metal/semiconductor interface is highly dependent on the relative positions of the Fermi level of the metal and the semiconductor band edges, as well as on the energy levels and concentrations of defect states in the band gap. Since using suitable electrodes is one of the easiest

Received: February 22, 2021
Revised: May 27, 2021
Published: June 10, 2021

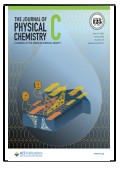

https://doi.org/10.1021/acs.jpcc.1c01612
J. Phys. Chem. C 2021, 125, 13551−13559

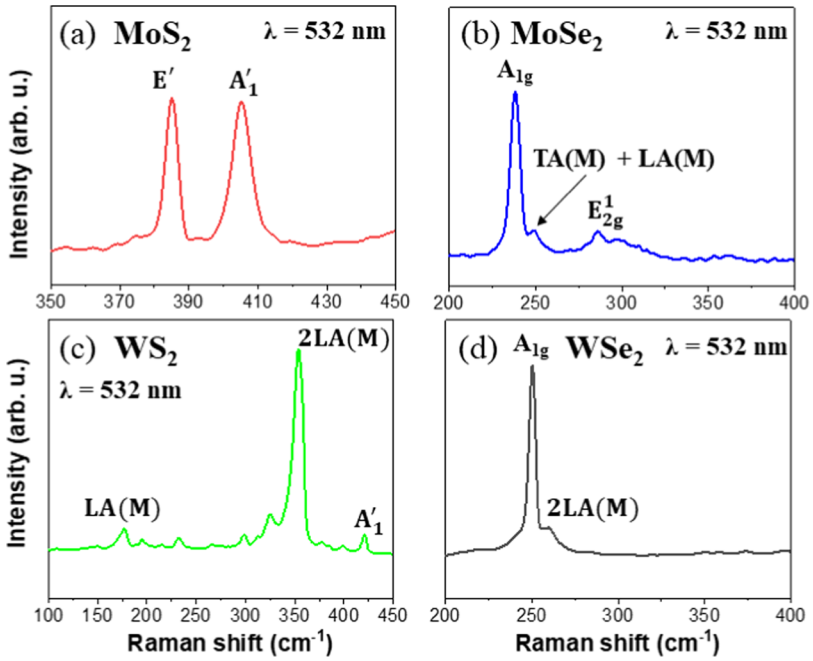

Figure 1. Raman spectrum measurements of monolayer MoS_2 (a), $MoSe_2$ (b), WS_2 (c), and WSe_2 (d).

ways to improve the performance of semiconductor devices and avoid unwanted losses due to, for example, a Schottky barrier, it is important to investigate if and how different substrates affect the energy-level alignment. Spatially resolved work function measurements were carried out under ambient conditions. Therefore, the results are relevant for devices that are fabricated by layer transfer of few-layer TMDs onto prepatterned metal electrodes in air.

2. METHODS AND MATERIALS

TMD 2D crystals were fabricated by chemical vapor deposition (CVD) on SiO_2/Si substrates. The atomic force microscopy (AFM) images of all studied materials on SiO_2/Si before the transfer can be found in the Supporting Information 1. Transfer of the TMDs, typically containing single-layer crystals and a smaller number of few-layer crystals, was done using a poly(methyl methacrylate) (PMMA)-assisted transfer process.[25] We used one-side-polished Si wafers (n-type, ⟨100⟩ orientation) covered with 20 nm thick sputtered Al or Au layers as substrates for the transferred TMDs. Since the experiments (in particular, layer transfer) were performed in ambient conditions, the Au surfaces were passivated by mild UV−ozone treatment to maintain a stable work function, which is at a somewhat higher value than that for unpassivated gold (our previous experiment has shown that polycrystalline gold surfaces that are passivated with UV−ozone treatment and subsequently handled in air have a higher work function than gold surfaces that were not treated in this way). Since Al oxidizes naturally in air, further passivation is not needed. The oxide layers involved are very thin (about 1 nm for Al, much thinner for Au), such that they do not hamper KPFM measurements. The TMD layers were covered by a PMMA layer on top as a support for transfer, which also serves to protect the TMDs from direct contact with ambient gases. It was removed right before the characterization of the samples.

Kelvin Probe Force Microscopy (KPFM) measurements were carried out to investigate the energy-level alignment at the metal/TMD interfaces, via contact potential measurements. To verify the thickness of the deposited TMD crystals before transfer, Raman spectroscopy (Bruker, Inc., SENTERRA Dispersive Raman Microscope) was employed. After transfer, the thickness was checked once again with AFM measurements. Mono- (1L), bi- (2L), or trilayer (3L) regions in transferred samples are identified by thickness measurements obtained from AFM topography images.

AFM/KPFM measurements were conducted using a Bruker Dimension Icon atomic force microscope in ambient conditions. The microscope has a closed feedback loop that improves the accuracy of force−distance measurements. The potential map was compared with the topography image to identify the number of layers in a TMD crystal. A heavily n-doped Si cantilever (resistivity = 0.01−0.025 Ω cm) with an aluminum coating (μMasch, HQ:NSC36/Al BS) was used with a resonance frequency of 90 kHz and a force constant of 1 N/m. The FM-KPFM mode was used (modulation frequency, 4 kHz; drive amplitude, 135 mV), and this one-pass method uses the frequency shift of the cantilever oscillation to detect the electrostatic force gradient. As the tip was grounded during the KPFM measurements, the contact potential difference (V_{CPD}) is determined by $V_{CPD} = \phi_s - \phi_{tip}/|e|$, with e being the elementary charge and ϕ_s and ϕ_{tip} are the work functions of the sample and tip, respectively. To detect the deflection of the tip cantilever, the KPFM instrument employs a laser diode that emits light with wavelengths of 650−695 nm, corresponding to an average photon energy of 1.85 eV. This exceeds the band gap of the studied materials, which could lead to the generation of free charge carriers within the TMD crystals and therefore possibly affect the KPFM measurements. Most of the incident light is reflected by the cantilever, and monolayer MoS_2 adsorbs less than 2% of the incident light with a wavelength of about 675 nm.[26] For the other TMD layers, the absorption at that wavelength is similar (<2%). The Au and Al substrate layers are only 20 nm thick such that the reflection of light, which could enhance the generation of photocarriers, is weak. We therefore expect that the influence of the laser on the

https://doi.org/10.1021/acs.jpcc.1c01612
J. Phys. Chem. C 2021, 125, 13551−13559

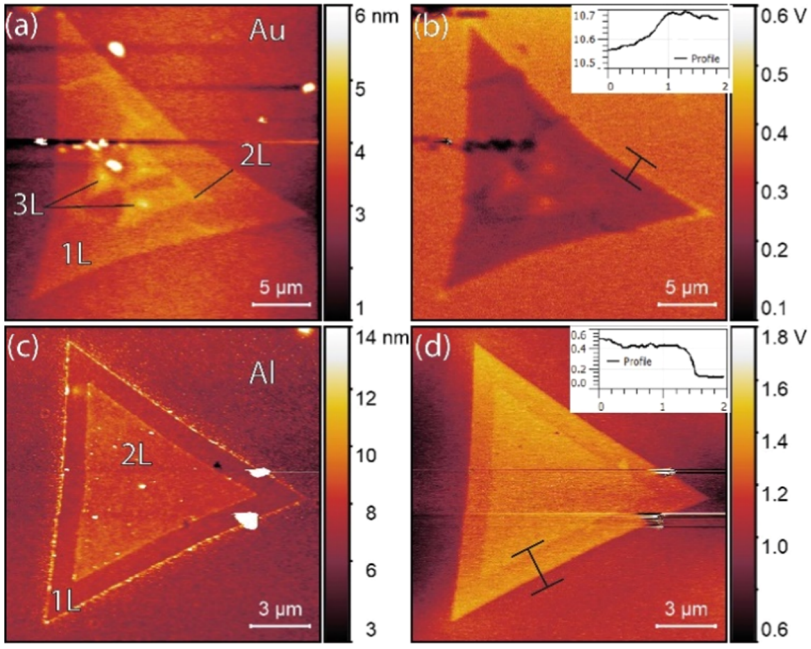

Figure 2. Mono-, double-, and triple-layer crystal of MoS_2: (a), (b) Au substrate and (c), (d) Al substrate. (a), (c) AFM topography map. (b), (d) Surface potential map. Insets in (b) and (d) show the line profile along designated area.

generation of charge carriers and, in turn, on the contact potential measurement is limited.

Ultraviolet photoelectron spectroscopy (UPS) in ultrahigh vacuum (10^{-9} mbar) using a He discharge UV lamp (He I line at 21.21 eV) was performed to verify the WFs of the uncovered substrates.

Previous reports have addressed the stability of TMD monolayers, in particular, of the degradation of selenide compounds.[23,24] To avoid degradation as much as possible, samples have been transported in an Ar environment and stored under vacuum in a desiccator. All presented results have been measured within 3 weeks after sample preparation.

3. RESULTS AND DISCUSSION

UPS measurements of bare substrates (Au and Al), using the well-established method of determining the secondary electron cutoff in UPS spectra, provided the WF values of 4.7 and 3.9 eV for Au and Al, respectively (Supporting Information Figure S2). The value for Au is lower than the work function of atomically clean polycrystalline Au (~5.2 eV)[27] due to exposure to air and UV−ozone plasma passivation of the surface. We have not noticed high impact of ambient conditions on the WFs of our samples. We compared UPS results that have been obtained in UHV to KPFM results in ambient conditions. Using a graphite sample with a known and stable WF value as a reference, we could compensate for the tip WF drift in KPFM measurements and determine the WFs of Al and Au using contact potential measurements. KPFM so-obtained results of the WF for Al and Au yielded 3.8 and −4.7 eV, respectively. We considered the UPS measurements to be more reliable since they are absolute and do not require any corrections and used the WF values from UPS for further calculations. To get a better understanding of how ambient conditions influence surface potential measurements,[28,29] we conducted humidity tests (Supporting Information 3). A minor impact was observed on the collected data at different humidity levels. Dry nitrogen as well as nitrogen rich with water vapor was applied to simulate extreme cases. The surface potential difference between gold and a $MoSe_2$ monolayer with dry nitrogen (10% RH) was measured to be 150 mV, 100 mV

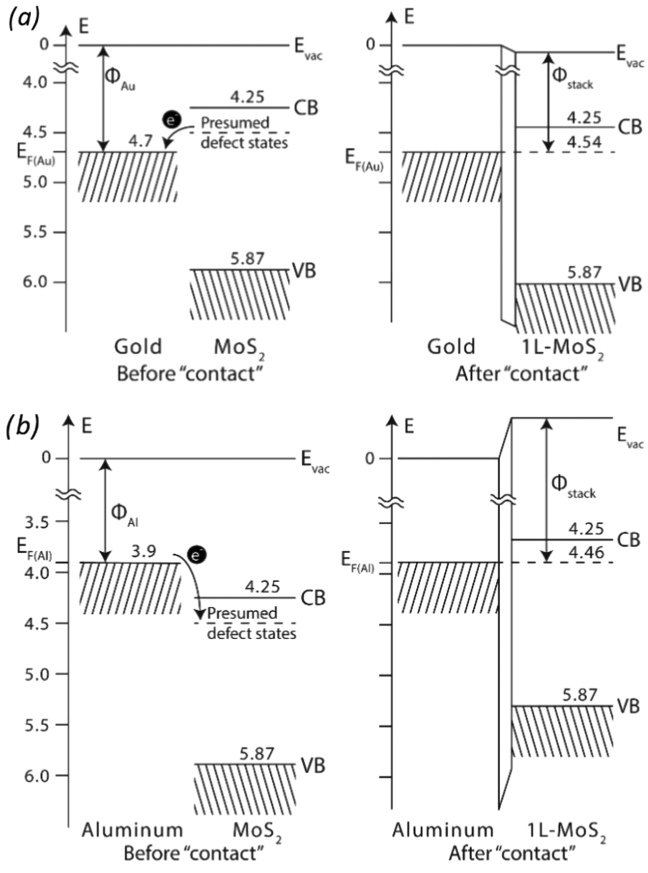

Figure 3. Band alignment before and after contact of (a) MoS_2 and Au and (b) MoS_2 and Al. The direction of electron transfer between the materials that occurs once contact is made is indicated by arrows.

https://doi.org/10.1021/acs.jpcc.1c01612
J. Phys. Chem. C 2021, 125, 13551−13559

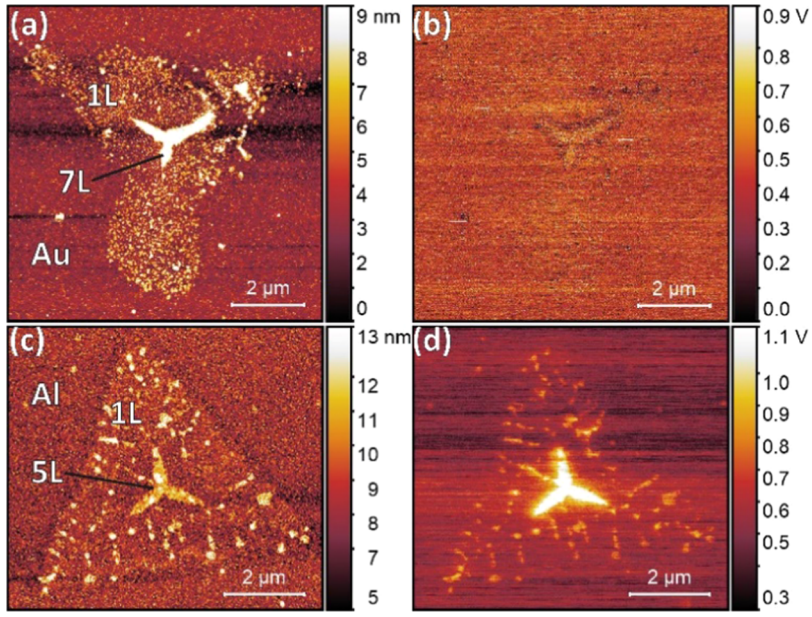

Figure 4. Monolayer crystal (with multilayer center) of WSe_2: (a), (b) Au substrate and (c), (d) Al substrate. (a), (c) AFM topography map. (b), (d) Surface potential map.

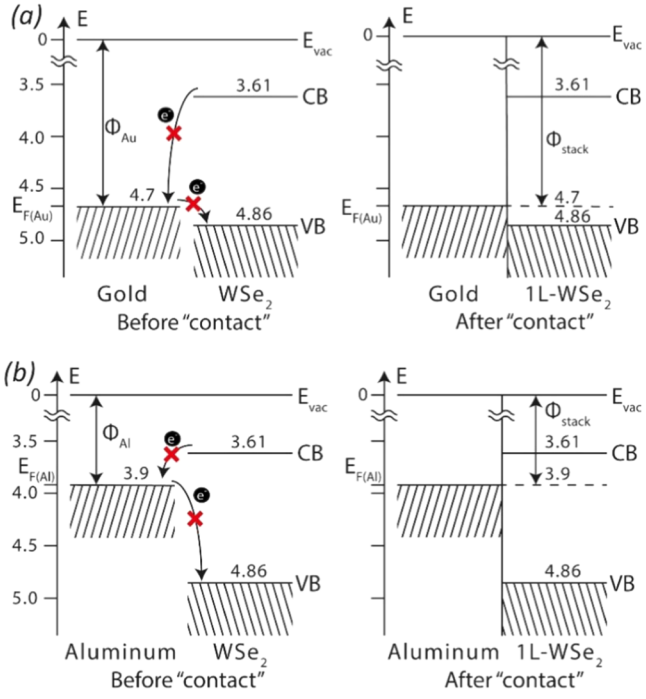

Figure 5. Band alignment before and after contact of (a) WSe_2 and Au and (b) WSe_2 and Al.

at ambient conditions (RH = 35%), and slightly less than 100 mV during high humidity scans (RH = 74%). Assuming the substrate WF to be the same for all samples (the substrates were cut from a single 100 mm wafer), the WF of the substrate with the TMDs on the top can be found from potential difference maps measured with KPFM.

In the following, we will describe each case of different contact behaviors, such as Schottky−Mott limit (WSe_2), Fermi-level pinning (MoS_2), or intermediate results depending on the substrates used, as in the cases of $MoSe_2$ and WS_2.

3.1. Raman Spectroscopy. In the MoS_2 Raman spectra (Figure 1a), the two characteristic modes[25] are E′ at 385 cm^{-1} (in-plane vibrations) and A_1' (out-of-plane vibrations) at 406 cm^{-1}. The difference between the two features A_1' − E′ is 21 cm^{-1}, which confirms that the MoS_2 crystals are monolayers.[25] A narrow E′-peak with a full width at half-maximum (FWHM) value of 4.7 cm^{-1} is found in MoS_2 spectra, which is an indication of a good crystallinity of MoS_2.[30]

In the $MoSe_2$ Raman spectra (Figure 1b), an A_{1g} mode at 241 cm^{-1} and an E_{2g} peak at 288 cm^{-1} as well as the combination modes of the longitudinal (LA(M)) and the transverse (TA(M)) at 250 cm^{-1} (originating from the vicinity of the high-symmetry M point of the $MoSe_2$ Brillouin zone)[31] show the formation of monolayer $MoSe_2$.[31,32]

In the WS_2 Raman spectra (Figure 1c), the LA(M) = 176 cm^{-1} (longitudinal acoustic mode), 2LA(M) = 353 cm^{-1} (second-order longitudinal acoustic mode), and A_1' = 420 cm^{-1} peaks are observable.[25] For monolayer WS_2 crystals, the 2LA(M) peak shows a particularly high intensity[30] when using 532 nm excitation, as can be seen in Figure 1c.

In the WSe_2 Raman spectra (Figure 1d), an A_{1g} peak at 250 cm^{-1} and a recognizable shoulder at 259 cm^{-1} (2LA(M) mode) can be seen,[33] which confirms that the WSe_2 crystals are monolayers.[34]

3.2. Fermi-Level Pinning: MoS_2. MoS_2 crystals, as all other TMD samples in this work, are made using a CVD process, which provides a large coverage with crystallite size ranging from a few μm to a maximum of 100 μm. As the Raman data show, the samples consist of predominantly monolayer crystals, with minor contributions of at most three layers. In the following, we use the notations 1L, 2L, and 3L to indicate monolayers, bilayers, and trilayers, respectively. MoS_2 crystals unavoidably contain defects. Defects in monolayers of MoS_2 and WS_2, produced in the same laboratory and under the same conditions, have been studied previously.[10] The areal density of defects in ML-MoS_2 is about 0.8 nm^{-2}, and they mostly consist of single S vacancies, while double S_2 vacancies amount to ∼8.5% of the total defect density. Although MoS_2

https://doi.org/10.1021/acs.jpcc.1c01612
J. Phys. Chem. C 2021, 125, 13551−13559

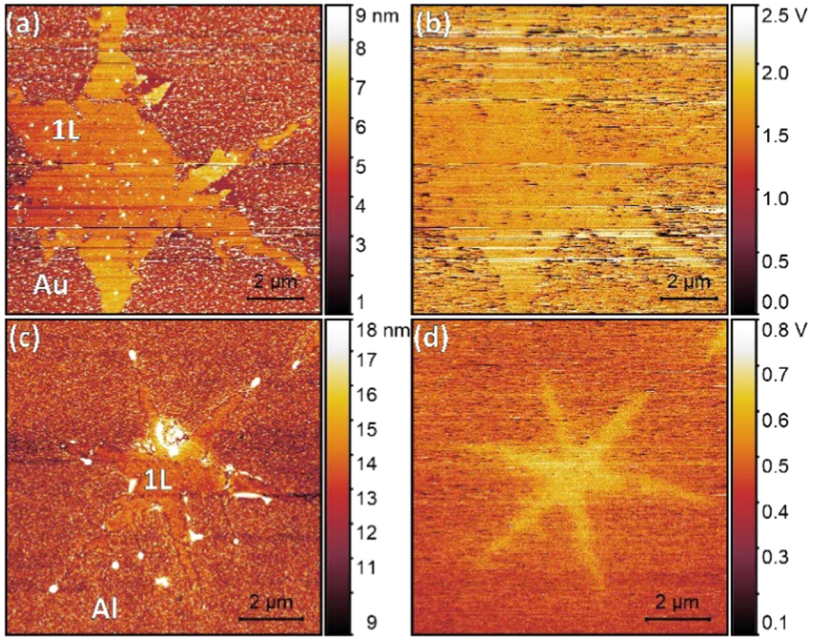

Figure 6. Monolayer crystal of $MoSe_2$: (a), (b) Au substrate and (c), (d) Al substrate. (a), (c) AFM topography map. (b), (d) Surface potential map.

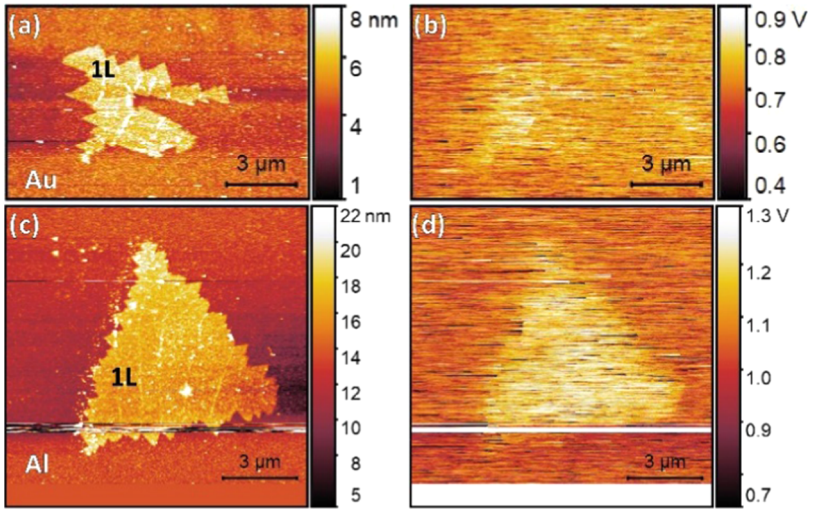

Figure 7. Monolayer crystal of WS_2: (a), (b) Au substrate and (c), (d) Al substrate. (a), (c) AFM topography map. (b), (d) Surface potential map.

layers exfoliated from bulk crystals may have lower defect density, CVD growth offers significant advantages regarding scalability and is thus of great interest for future applications.

The average difference between the surface potential of a 1L MoS_2 crystal and that of the surrounding Au "background" is −150 mV, which corresponds to a WF of the MoS_2 monolayer on Au of 4.54 ± 0.03 eV. Similar measurements of 1L of the same CVD MoS_2 transferred to an Al substrate show a contact potential difference of +580 mV, which sets the WF of the MoS_2 monolayer on Al at 4.46 ± 0.09 eV. Since these WF values are nearly the same, it can be concluded that for MoS_2 monolayers, the substrate Fermi level is strongly pinned at about 4.5 eV below the vacuum level (Figure 2).

In addition to 1L MoS_2 crystals, double- and triple-layer regions were observed, often occurring within the same crystal. Although the WFs measured on 1L and 2L MoS_2 are essentially the same, the difference with 3L regions is clearly visible in the contact potential maps but never exceeds about +0.1 V.

These results are similar to previous reports that showed a monotonic increase of the WF of MoS_2 with an increasing number of layers.[4,5] Note that those studies focused only on TMDs deposited by CVD processes without transfer, so these studies were conducted only on the growth substrate—SiO_2/Si. We attribute the observation of Fermi-level pinning to the exchange of electrons between the substrate Fermi level and defect states in the MoS_2, which results in an interfacial dipole that pins the Fermi level at a fixed value below the vacuum level.[35]

Figure 3 shows a simple diagram that depicts how the energy levels of the metals and the MoS_2 align after a contact has been made. The values of the conduction band minimum (CB) and valance band maximum (VB) are taken from a publication by Kang et al.[18] Our experimental data suggests that there are

https://doi.org/10.1021/acs.jpcc.1c01612
J. Phys. Chem. C 2021, 125, 13551−13559

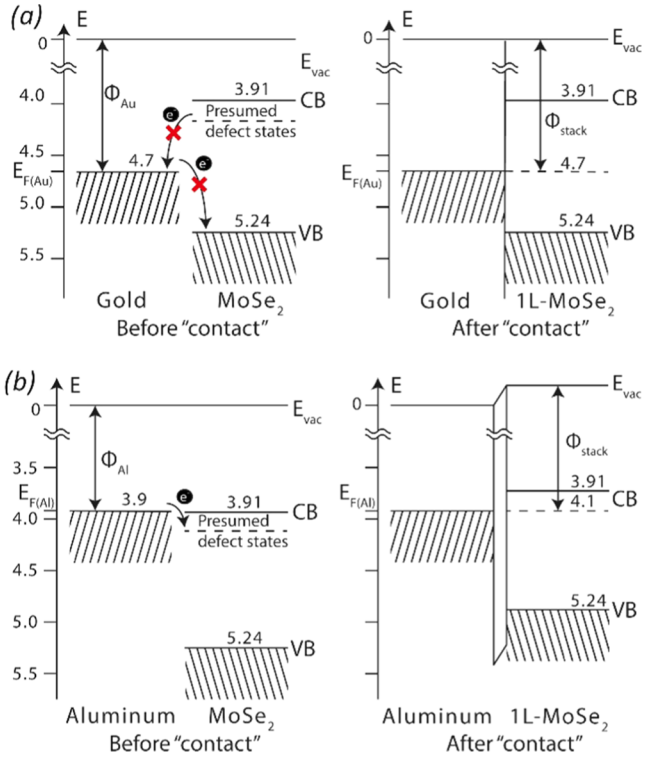

Figure 8. Band alignment before and after contact of (a) $MoSe_2$ and Au and (b) $MoSe_2$ and Al.

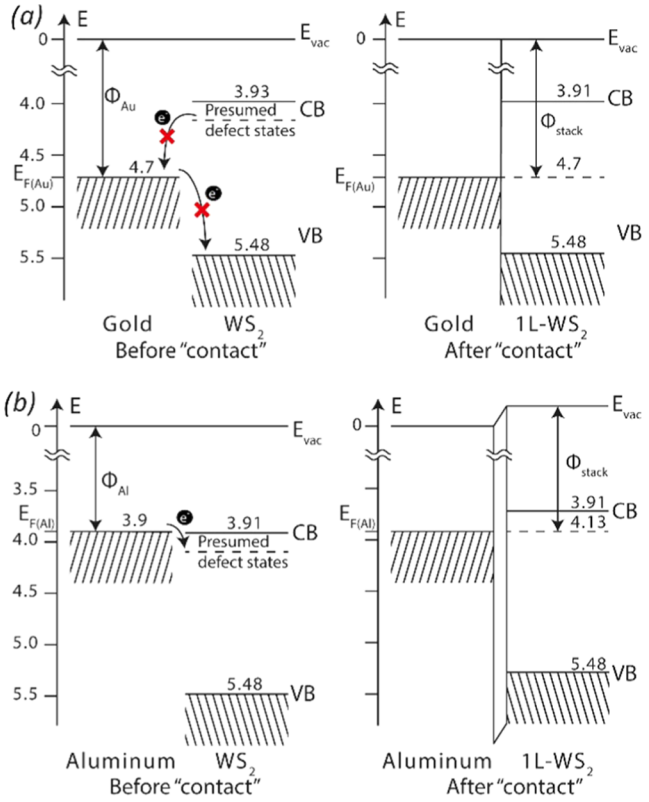

Figure 9. Band alignment before and after contact of (a) WS_2 and Au and (b) WS_2 and Al.

defect states within the band gap that could serve either as donors or as acceptors of electrons.[36] Similar behavior for these types of defects was previously reported by Song et al.[37]

The Fermi energy of both stacks (MoS_2/Au and MoS_2/Al) is pinned at that level. In the diagrams, the potential variations at the interface are represented as is typical for "interface dipoles" rather than "band bending," consistent with the notion that the potential variation has to take place within the MoS_2 monolayer such that there cannot be an extended depletion region.

3.3. Schottky–Mott Limit: WSe_2. Figure 4 shows the topography and potential maps of WSe_2 on Au and Al. 1L crystals do not provide any contact potential contrast on both substrates. Visible features in the potential map of a single layer on Al occur where height variations are observed in the topography maps. These height variations may be associated with wrinkles and/or small multilayer regions in the center of the structure, presumably where the WSe_2 crystal nucleated, one can observe a thicker region. The thickness of this central part and similar regions in different structures, according to our estimations, varies from ∼5 to ∼7 layers. Such a high number of layers provides a clear potential difference for WSe_2 on Al substrates: the difference in the contact potential is about +300 mV, which corresponds to a higher WF equal to 4.19 ± 0.07 eV in the central region.

On Au, no clear surface potential difference is observed. Instead, few-layer regions of WSe_2 on Au can be recognized in the potential maps because of their outlines, but they do not exhibit any potential difference with the substrate within the experimental error. The darker outlines might be artefacts caused by the significant step edges occurring at the transition from 1 to 7 layers.

The diagrams in Figure 5 depict how the energy levels align for WSe_2 monolayers on Au and Al. The observation of a constant WF on or off the WSe_2 monolayer indicates that charge transfer does not take place at the interface, which represents the Schottky–Mott limit. Such an observation can be explained by the absence or low concentration of defect states within the band gap. We stress that the Schottky–Mott limit holds when there is (almost) no charge transfer between the metal substrate and the TMDs. This is the case when the Fermi energy of the metal resides in the band gap of the TMD, with no (or very few) in-gap defect states present that could facilitate charge transfer. Such behavior is well described in ref 11.

3.4. Intermediate Case: WS_2 and $MoSe_2$. Transferred samples of $MoSe_2$ and WS_2 exhibit not only similar electrical contact properties but also similar topography. Both samples only contain single-layer regions (Figures 6 and 7).

On Au, both $MoSe_2$ and WS_2 are almost not visible in the surface potential maps. In the case of $MoSe_2$, the maximum WF difference is 0.1 eV and another effect that can be noticed is a smoother signal in comparison to the signal measured on the bare Au surface, which might be attributed to different tip/sample interactions and the presence of PMMA residues. PMMA (950 kDa) was used as a support layer for transfer of the TMD crystals and cannot be fully removed. The residues appear as small protrusions in the AFM topography image (Figures 6a,c and 7a), which look similar to previously reported PMMA residues on the surface of CVD-grown graphene.[38] In spite of the difference in potential fluctuations on and off the $MoSe_2$ crystals, the average difference of the potentials measured on both monolayers and bare Au is smaller than 50 mV, which is within the noise error. In contrast to this, the potential observed on $MoSe_2$ and WS_2 crystals on Al is significantly higher than that on the adjacent bare

https://doi.org/10.1021/acs.jpcc.1c01612
J. Phys. Chem. C 2021, 125, 13551−13559

Table 1. Work Functions Measured on Top of Various TMD Crystals Located at Au and Al Surfaces[a]

	gold (WF = 4.7 eV), eV			aluminum (WF = 3.9 eV), eV		
	1 layer	2 layers	3 or more L	1 layer	2 layers	3 or more L
MoS_2	4.54 ± 0.03	4.58 ± 0.05	4.62 ± 0.06	4.46 ± 0.09	4.48 ± 0.07	4.60 ± 0.01
$MoSe_2$	**4.71 ± 0.02**	N/A	N/A	4.11 ± 0.07	N/A	N/A
WS_2	**4.75 ± 0.02**	N/A	N/A	4.13 ± 0.07	N/A	N/A
WSe_2	**4.70 ± 0.01**	N/A	**4.69 ± 0.03**	**3.92 ± 0.04**	N/A	4.19 ± 0.07

[a]All relative values have been determined by KPFM measurements, whereas absolute values are based on the WF of the substrate as obtained from UPS measurements. Bold values represent the Schottky−Mott limit behavior, when there is almost no potential difference between the substrates and TMD. Error values correspond to standard deviations.

substrate. The potential difference is highly similar in both cases and is about 250 mV. That sets the work function of the monolayer-$MoSe_2$/Al stack to 4.11 ± 0.07 eV, and that of the monolayer-WS_2/Al stack to 4.13 ± 0.07 eV.

The diagrams displayed in Figures 8 and 9 depict the energy-level alignment for both these cases. It can be concluded that $MoSe_2$ and WS_2 behave according to the Schottky−Mott limit in the case of transfer to an Au substrate: no work function difference was observed, which implies that no interfacial charge transfer between $MoSe_2$ and Au occurs.

For the same materials located on an Al substrate, the Fermi level is pinned at about 4.1 eV, i.e., a few tenths of electron volts above the work function of Al. A possible explanation could be the following: defect states act only as acceptors for electrons from Al, such that its Fermi level becomes pinned, while electron donation to Au does not take place, resulting in band alignment according to the Schottky−Mott limit. Such a scenario could occur if the defect states in the band gap are predominantly unoccupied states.

4. CONCLUSIONS

In conclusion, we studied several members of the family of transition-metal dichalcogenides, MoS_2, $MoSe_2$, WS_2, and WSe_2, transferred to Au and Al substrates. All of the measured work functions of the different stacks are provided in Table 1. The results show different types of metal−semiconductor junctions. For MoS_2, the substrate Fermi level is pinned at the energy level of the defect states within the band gap, at about 4.5 eV. It is noteworthy that these states serve both as donors and acceptors of electrons. Fermi-level pinning is also observed in the cases of $MoSe_2$ and WS_2, but only when these materials are transferred to Al. This is consistent with the notion that there are defect states in the band gap that serve as acceptors of electrons from Al but no states that donate electrons to Au.

The Schottky−Mott limit behavior is observed for WSe_2: no charge transfer appeared after transfer to either Au or Al. We cannot claim that these samples are defect free but potentially the defect concentration is not high enough to result in significant charge transfer.

Our study provides valuable information on metal−TMD interactions, which can help in the future design of electronic devices based on these materials. One can draw the conclusion that the adjustment of the electrode material in the case of MoS_2-based devices will not provide any difference in performance due to the strongly pinned Fermi level. On the other hand, WSe_2-based devices can be enhanced by designating suitable electrodes. To a certain extent, this also applies to $MoSe_2$ and WS_2 monolayers, for which Fermi-level pinning was only observed for TMDs located on Al substrates.

■ ASSOCIATED CONTENT

Supporting Information

The Supporting Information is available free of charge at https://pubs.acs.org/doi/10.1021/acs.jpcc.1c01612.

Additional figures and tables; UPS measurements; work function dependence on ambient humidity (PDF)

■ AUTHOR INFORMATION

Corresponding Author

Pavel A. Markeev − *MESA+ Institute for Nanotechnology, University of Twente, 7500 AE Enschede, The Netherlands;* orcid.org/0000-0002-5445-1224; Email: p.markeev@utwente.nl

Authors

Emad Najafidehaghani − *Institute of Physical Chemistry, Abbe Center of Photonics, Friedrich Schiller University, 07743 Jena, Germany*

Ziyang Gan − *Institute of Physical Chemistry, Abbe Center of Photonics, Friedrich Schiller University, 07743 Jena, Germany*

Kai Sotthewes − *MESA+ Institute for Nanotechnology, University of Twente, 7500 AE Enschede, The Netherlands;* orcid.org/0000-0003-2073-6958

Antony George − *Institute of Physical Chemistry, Abbe Center of Photonics, Friedrich Schiller University, 07743 Jena, Germany;* orcid.org/0000-0002-9317-5920

Andrey Turchanin − *Institute of Physical Chemistry, Abbe Center of Photonics, Friedrich Schiller University, 07743 Jena, Germany;* orcid.org/0000-0003-2388-1042

Michel P. de Jong − *MESA+ Institute for Nanotechnology, University of Twente, 7500 AE Enschede, The Netherlands;* orcid.org/0000-0003-3668-9121

Complete contact information is available at: https://pubs.acs.org/10.1021/acs.jpcc.1c01612

Notes

The authors declare no competing financial interest.

■ ACKNOWLEDGMENTS

The authors acknowledge financial support from the European Union's Horizon 2020 research and innovation program FLAG-ERA, joint with the Dutch Research Council (NWO), and Deutsche Forschungsgemeinschaft (DFG—German Research Foundation) under grant nos. 680-91-313 (NWO) and TU149/9-1 (DFG).

■ REFERENCES

(1) Schottky, W. Zur Halbleitertheorie Der Sperrschicht- Und Spitzengleichrichter. *Z, Phys.* **1939**, *113*, 367−414.

(2) Sze, S. M. *Semiconductor Devices Physics and Technology*; 2nd ed.; Wiley: New York, 2002; pp 1−4.
(3) Bardeen, J. Surface States and Rectification at a Metal Semi-Conductor Contact. *Phys. Rev.* **1947**, *71*, No. 717.
(4) Tamulewicz, M.; Kutrowska-Girzycka, J.; Gajewski, K.; Serafińczuk, J.; Sierakowski, A.; Jadczak, J.; Bryja, L.; Gotszalk, T. P. Layer Number Dependence of the Work Function and Optical Properties of Single and Few Layers MoS2: Effect of Substrate. *Nanotechnology* **2019**, *30*, No. 245708.
(5) Choi, S. H.; Shaolin, Z.; Yang, W. Layer-Number-Dependent Work Function of MoS2 Nanoflakes. *J. Korean Phys. Soc.* **2014**, *64*, 1550−1555.
(6) Li, F.; Qi, J.; Xu, M.; Xiao, J.; Xu, Y.; Zhang, X.; Liu, S.; Zhang, Y. Layer Dependence and Light Tuning Surface Potential of 2D MoS2 on Various Substrates. *Small* **2017**, *13*, No. 1603103.
(7) Sohn, A.; Moon, H.; Kim, J.; Seo, M.; Min, K. A.; Lee, S. W.; Yoon, S.; Hong, S.; Kim, D. W. Band Alignment at Au/MoS2 Contacts: Thickness Dependence of Exfoliated Flakes. *J. Phys. Chem. C* **2017**, *121*, 22517−22522.
(8) Manzeli, S.; Ovchinnikov, D.; Pasquier, D.; Yazyev, O. V.; Kis, A. 2D Transition Metal Dichalcogenides. *Nat. Rev. Mater.* **2017**, *2*, No. 17033.
(9) Hong, J.; Jin, C.; Yuan, J.; Zhang, Z. Atomic Defects in Two-Dimensional Materials: From Single-Atom Spectroscopy to Functionalities in Opto-/Electronics, Nanomagnetism, and Catalysis. *Adv. Mater.* **2017**, *29*, No. 1606434.
(10) George, A.; Fistul, M. V.; Gruenewald, M.; Kaiser, D.; Lehnert, T.; Mupparapu, R.; Neumann, C.; Hübner, U.; Schaal, M.; Masurkar, N.; Arava, L. M. R.; Staude, I.; Kaiser, U.; Fritz, T.; Turchanin, A. Giant Persistent Photoconductivity in Monolayer MoS2 Field-Effect Transistors. *npj 2D Mater. Appl.* **2021**, *5*, No. 15.
(11) Liu, Y.; Guo, J.; Zhu, E.; Liao, L.; Lee, S. J.; Ding, M.; Shakir, I.; Gambin, V.; Huang, Y.; Duan, X. Approaching the Schottky-Mott Limit in van Der Waals Metal-Semiconductor Junctions. *Nature* **2018**, *557*, 696−700.
(12) Kang, S.; Lee, D.; Kim, J.; Capasso, A.; Kang, H. S.; Park, J. W.; Lee, C. H.; Lee, G. H. 2D Semiconducting Materials for Electronic and Optoelectronic Applications: Potential and Challenge. *2D Mater.* **2020**, *7*, No. 022003.
(13) Li, M.; Lan, F.; Yang, W.; Ji, Z.; Zhang, Y.; Xi, N.; Xin, X.; Jin, X.; Li, G. Influence of MoS2-Metal Interface on Charge Injection: A Comparison between Various Metal Contacts. *Nanotechnology* **2020**, *31*, No. 395713.
(14) Kahn, A. Fermi Level, Work Function and Vacuum Level. *Mater. Horiz.* **2016**, *3*, 7−10.
(15) Gupta, A.; Sakthivel, T.; Seal, S. Recent Development in 2D Materials beyond Graphene. *Prog. Mater. Sci.* **2015**, *73*, 44−126.
(16) Ataca, C.; Şahin, H.; Ciraci, S. Stable, Single-Layer MX 2 Transition-Metal Oxides and Dichalcogenides in a Honeycomb-like Structure. *J. Phys. Chem. C* **2012**, *116*, 8983−8999.
(17) Jiang, H. Electronic Band Structures of Molybdenum and Tungsten Dichalcogenides by the GW Approach. *J. Phys. Chem. C* **2012**, *116*, 7664−7671.
(18) Kang, J.; Tongay, S.; Zhou, J.; Li, J.; Wu, J. Band Offsets and Heterostructures of Two-Dimensional Semiconductors. *Appl. Phys. Lett.* **2013**, *102*, No. 012111.
(19) Gong, C.; Zhang, H.; Wang, W.; Colombo, L.; Wallace, R. M.; Cho, K. Band Alignment of Two-Dimensional Transition Metal Dichalcogenides: Application in Tunnel Field Effect Transistors. *Appl. Phys. Lett* **2013**, *103*, No. 053513.
(20) Rasmussen, F. A.; Thygesen, K. S. Computational 2D Materials Database: Electronic Structure of Transition-Metal Dichalcogenides and Oxides. *J. Phys. Chem. C* **2015**, *119*, 13169−13183.
(21) Özçelik, V. O.; Azadani, J. G.; Yang, C.; Koester, S. J.; Low, T. Band Alignment of Two-Dimensional Semiconductors for Designing Heterostructures with Momentum Space Matching. *Phys. Rev. B* **2016**, *94*, No. 35125.
(22) Fang, H.; Battaglia, C.; Carraro, C.; Nemsak, S.; Ozdol, B.; Kang, J. S.; Bechtel, H. A.; Desai, S. B.; Kronast, F.; Unal, A. A.; Conti, G.; Conlon, C.; Palsson, G. K.; Martin, M. C.; Minor, A. M.; Fadley, C. S.; Yablonovitch, E.; Maboudian, R.; Javey, A. Strong Interlayer Coupling in van Der Waals Heterostructures Built from Single-Layer Chalcogenides. *Proc. Natl. Acad. Sci. U.S.A.* **2014**, *111*, 6198−6202.
(23) Wilson, N. R.; Nguyen, P. V.; Seyler, K.; Rivera, P.; Marsden, A. J.; Laker, Z. P. L.; Constantinescu, G. C.; Kandyba, V.; Barinov, A.; Hine, N. D. M.; Xu, X.; Cobden, D. H. Determination of Band Offsets, Hybridization, and Exciton Binding in 2D Semiconductor Heterostructures. *Sci. Adv.* **2017**, *3*, No. e1601832.
(24) Keyshar, K.; Berg, M.; Zhang, X.; Vajtai, R.; Gupta, G.; Chan, C. K.; Beechem, T. E.; Ajayan, P. M.; Mohite, A. D.; Ohta, T. Experimental Determination of the Ionization Energies of MoSe 2, WS 2, and MoS 2 on SiO 2 Using Photoemission Electron Microscopy. *ACS Nano* **2017**, *11*, 8223−8230.
(25) George, A.; Neumann, C.; Kaiser, D.; Mupparapu, R.; Lehnert, T.; Hübner, U.; Tang, Z.; Winter, A.; Kaiser, U.; Staude, I.; Turchanin, A. Controlled Growth of Transition Metal Dichalcogenide Monolayers Using Knudsen-Type Effusion Cells for the Precursors. *J. Phys. Mater.* **2019**, *2*, No. 016001.
(26) Bernardi, M.; Palummo, M.; Grossman, J. C. Extraordinary Sunlight Absorption and One Nanometer Thick Photovoltaics Using Two-Dimensional Monolayer Materials. *Nano Lett.* **2013**, *13*, 3664−3670.
(27) Yeo, Y. C.; King, T. J.; Hu, C. Metal-Dielectric Band Alignment and Its Implications for Metal Gate Complementary Metal-Oxide-Semiconductor Technology. *J. Appl. Phys.* **2002**, *92*, 7266−7271.
(28) Kim, J. H.; Lee, J.; Kim, J. H.; Hwang, C. C.; Lee, C.; Park, J. Y. Work Function Variation of MoS2 Atomic Layers Grown with Chemical Vapor Deposition: The Effects of Thickness and the Adsorption of Water/Oxygen Molecules. *Appl. Phys. Lett.* **2015**, *106*, No. 251606.
(29) Feng, Y.; Zhang, K.; Li, H.; Wang, F.; Zhou, B.; Fang, M.; Wang, W.; Wei, J.; Wong, H. S. P. In Situ Visualization and Detection of Surface Potential Variation of Mono and Multilayer MoS2 under Different Humidities Using Kelvin Probe Force Microscopy. *Nanotechnology* **2017**, *28*, No. 295705.
(30) Zhang, X.; Qiao, X. F.; Shi, W.; Wu, J. B.; Jiang, D. S.; Tan, P. H. Phonon and Raman Scattering of Two-Dimensional Transition Metal Dichalcogenides from Monolayer, Multilayer to Bulk Material. *Chem. Soc. Rev.* **2015**, *44*, 2757−2785.
(31) Soubelet, P.; Bruchhausen, A. E.; Fainstein, A.; Nogajewski, K.; Faugeras, C. Resonance Effects in the Raman Scattering of Monolayer and Few-Layer MoSe2. *Phys. Rev. B* **2016**, *93*, No. 155407.
(32) Tonndorf, P.; Schmidt, R.; Böttger, P.; Zhang, X.; Börner, J.; Liebig, A.; Albrecht, M.; Kloc, C.; Gordan, O.; Zahn, D. R. T.; Michaelis de Vasconcellos, S.; Bratschitsch, R. Photoluminescence Emission and Raman Response of Monolayer MoS_2, MoSe_2, and WSe_2. *Opt. Express* **2013**, *21*, 4908.
(33) Huang, J. K.; Pu, J.; Hsu, C. L.; Chiu, M. H.; Juang, Z. Y.; Chang, Y. H.; Chang, W. H.; Iwasa, Y.; Takenobu, T.; Li, L. J. Large-Area Synthesis of Highly Crystalline WSe2 Monolayers and Device Applications. *ACS Nano* **2014**, *8*, 923−930.
(34) Sahin, H.; Tongay, S.; Horzum, S.; Fan, W.; Zhou, J.; Li, J.; Wu, J.; Peeters, F. M. Anomalous Raman Spectra and Thickness-Dependent Electronic Properties of WSe2. *Phys. Rev. B: Condens. Matter Mater. Phys.* **2013**, *87*, No. 165409.
(35) Kim, C.; Moon, I.; Lee, D.; Choi, M. S.; Ahmed, F.; Nam, S.; Cho, Y.; Shin, H. J.; Park, S.; Yoo, W. J. Fermi Level Pinning at Electrical Metal Contacts of Monolayer Molybdenum Dichalcogenides. *ACS Nano* **2017**, *11*, 1588−1596.
(36) Hong, J.; Hu, Z.; Probert, M.; Li, K.; Lv, D.; Yang, X.; Gu, L.; Mao, N.; Feng, Q.; Xie, L.; Zhang, J.; Wu, D.; Zhang, Z.; Jin, C.; Ji, W.; Zhang, X.; Yuan, J.; Zhang, Z. Exploring Atomic Defects in Molybdenum Disulphide Monolayers. *Nat. Commun.* **2015**, *6*, No. 6293.
(37) Song, S. H.; Joo, M. K.; Neumann, M.; Kim, H.; Lee, Y. H. Probing Defect Dynamics in Monolayer MoS2 via Noise Nanospectroscopy. *Nat. Commun.* **2017**, *8*, No. 2121.

(38) Choi, W.; Shehzad, M. A.; Park, S.; Seo, Y. Influence of Removing PMMA Residues on Surface of CVD Graphene Using a Contact-Mode Atomic Force Microscope. *RSC Adv.* **2017**, *7*, 6943−6949.

https://doi.org/10.1021/acs.jpcc.1c01612
J. Phys. Chem. C 2021, 125, 13551−13559